2024 IEEE/RSJ International Conference on Intelligent Robots and Systems (IROS)
October 14-18, 2024. Abu Dhabi, UAE

Manta Ray-Inspired Soft Robotic Swimmer for High-speed and Multi-modal Swimming

Zefeng Xu, Jiaqiao Liang, and Yitong Zhou*

***Abstract*— Manta rays exhibit complex motion behavior through their flexible fins. This study proposes a novel manta ray-inspired soft robotic swimmer with bistable flapping wings for high-speed and multi-modal swimming. The wings are created with prestressed bistable composite and actuated by small McKibben artificial muscles. Pressurizing and depressurizing the McKibben actuators integrated into the flapping wings generates alternating snap-throughs between two stable states, yielding swimming. Experiments are set up and conducted to analyze how the robot responses vary as a function of input pressures and actuation frequencies for both bistable and monostable modes. Experimental results show that the highest swimming velocity is 0.58 body lengths (BL) per second (equivalent to 12.23 cm/s), and the maximum turning angle speed is 22.5° per second with a smaller turning radius by holding the fins in asymmetric positions for bistable modes. Multimodal swimming motions are achieved including forward and backward translating, turning, and flip-turning.**

I. Introduction

The manta rays have fast yet energy-efficient and exceptional maneuverability swimming mode propelled by curved, flexible flapping wings, which have a high propulsive efficiency of 89% [1]. Inspired by the motion and structural characteristics, multiple soft robotic swimmers utilizing flaps have been developed for eco-monitoring [2], deep-sea exploration [3], and aquaculture inspection [4].

In recent years, researchers have developed a series of flapping-wing soft manta ray robots [5], [6]. Liu et al. designed a manta ray robot with a soft material-based flapping wing that can swim forward continually with a speed of 0.17 BL/s [7]. Wang et al. developed a bionic manta ray robot that just provided turning by using flexible passive stereo bionic pectoral fins [8]. Sun et al. achieved a giant manta ray robot propelled by a 2D soft morphing actuator with the Mobuliform swimming mode [9]. However, these robots are limited to low velocity and swimming modal simplicity due to soft materials' low stiffness and viscosity. The development of fast and highly efficient aqueous underwater soft robots remains a grand challenge.

To address this challenge, a few researchers have incorporated bistable structures into flexible flapping wings [10]–[12], which allow rapid snap-throughs by releasing intrinsic stored energy instantaneously with relatively small forces [13], [14]. Furthermore, they require no energy to maintain stable states, hence improving energy efficiency. Such as Osorio et al. presented a pneumatically actuated manta ray soft robot flapping through locally independent deflections caused by bistable snap-through transitions [12]. Nevertheless, these studies were limited by the structural design and the actuation modes, which can only achieve forward translating and rotational motion. These few swimming modes prevent the utilization of manta-ray-like robotics in complex environments.

In our previous study, we proposed mechanically-prestressed pneumatically-driven bistable soft actuators [15], [16] based on Fluid Prestressed Composites (FPCs) with equilibrium curvatures. These actuators were used to develop crawlers [17] and grippers [18], which demonstrated advantages such as fast response time, lower energy consumption, and the ability to maintain their equilibrium shapes without external energy. Moreover, the stable shapes and stability of the soft actuators can be simply tailored by the magnitudes and directions of the prestress applied to the composite.

In this paper, we propose a novel manta ray-inspired soft robotic swimmer composed of two bistable flapping wings based on a mechanically prestressed composite for the first time. The bistable wings are simply created by pre-stretching crossed elastomer layers on both sides of a compliant thin plate, allowing for a simple structure, fast fabrication, and high potential for tailorable morphology. Lightweight McKibben artificial muscles are integrated on both sides of the wings for actuating snap-through of the wings, which have the advantages of low energy consumption, small size, and almost unaffected by underwater environment compared to shape memory alloy and dielectric elastomer actuators [19]. By controlling the pressure applied to different McKibben actuators, multimodal swimming motions can be achieved including forward and backward translating, turning, and flip-turning. Experiments are conducted to compare the swimming patterns of monostable and bistable swimming modes. This study not only provides a novel method for creating high-speed bistable soft swimming robots but also achieves more swimming modes compared to existing manta ray-like robots, proving the high potential for our proposed bistable soft robotic.

II. Methods of Soft Bistable Manta-Ray Robots

The overall design of the proposed swimming robot is shown in Fig. 1, which consists of one connector, and two flapping wings each integrated with two McKibben artificial muscles. Flapping wing design and swimming mechanism are detailed in the following sub-sections.

*This work was supported by the National Natural Science Foundation of China under Grant No. 62203174. *(Corresponding author: Yitong Zhou.)*

Zefeng Xu, Jiaqiao Liang, and Yitong Zhou are with the Shien-Ming Wu School of Intelligent Engineering, South China University of Technology, Guangzhou 511442, China, 202110190503@mail.scut.edu.cn; wiliangjiaqiao@mail.scut.edu.cn; zhouyitong@scut.edu.cn.

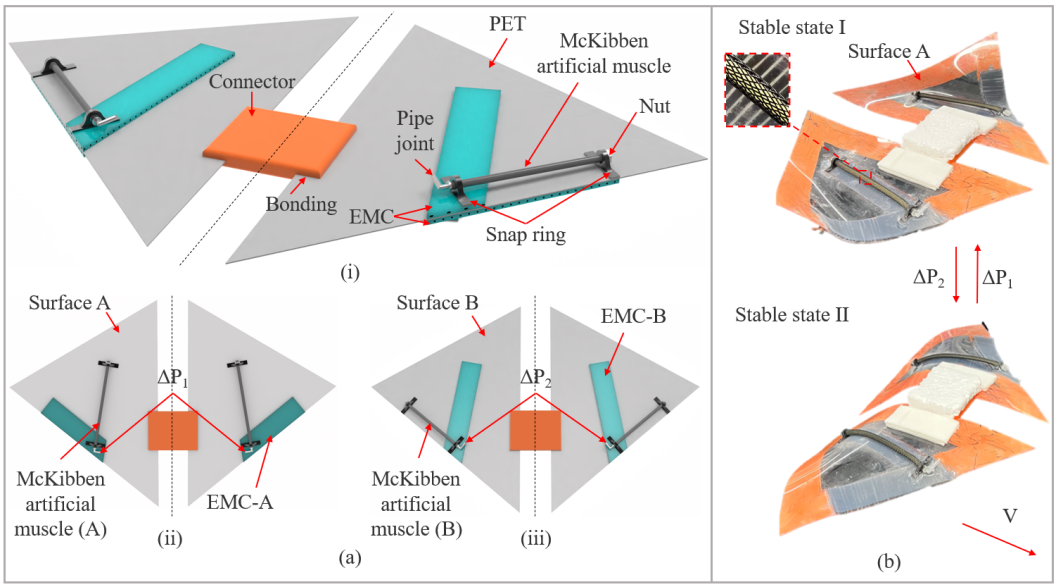

Fig. 1. Design and bistable shapes of the proposed soft bistable manta ray-inspired robot. (a) Schematic design of a soft bistable manta-ray robotic. (b) Rendered robot with stable states I and II. Pneumatic actuation of the McKibben artificial muscles (A) ($P_2 > 0$) in state II triggers the wing to snap to stable state I and vice versa. V represents the swimming direction.

A. *Flapping Wing Design*

Fig. 1(a) depicts the overall design of the manta ray-inspired robot, which is created by connecting two symmetrically positioned bistable pre-curved flapping wings via a 3D-printed connector. The wings can transition between the two stable states by applying pneumatic pressure to the McKibben artificial muscle to counteract the bending prestress within the Elastomer Matrix Composite (EMC) on the opposing sides of the wing, as illustrated in Fig. 1(b). The edges of the flapping wings are painted orange for easy differentiation from the environment.

The EMC layer is a fiber-reinforced elastomer composite, which is made by sandwiching unidirectional carbon fibers between two pre-cured silicone sheets [20]. This composite exhibits anisotropic stiffness, effectively restricting transverse shrinkage under longitudinal tensile load. As shown in Fig. 1(a), two EMC layers, including the EMC-A and EMC-B, are pre-stretched prior to bonding to the Polyethylene Terephthalate (PET) core layer, which generates the bistable composite plates with curvatures along the two EMCs' longitudinal directions in the flapping wing. EMC-A and EMC-B represent the EMC on the edge of surface A of the PET layer and the one at surface B, angled at 60°. The wing's shape and bistability can be tailored by customizing prestrain of the two EMCs and the dimensions of the core layer. Here, the proportion of pre-stretching is called prestrains. For instance, the prestrain value is defined as 40% when an EMC is pre-stretched to 140% of its initial length.

A McKibben artificial muscle is made using an embedded rubber tube and a fiber mesh, as shown in Fig. 1(b). The radial expansion of the tube is limited by the fiber mesh of the outer layer under pressurization, converting the pneumatic power into the pulling force of contraction. Hence, the controlled transition of the flapping wing between distinct stable states is enabled by the actuation of two separate McKibben artificial muscles. Snap rings are used at the ends of the muscles to secure them on the back of the EMC, while a nut serves as a fastening mechanism to avoid loosening of the muscle.

Compared to our previous bistable actuators proposed in [**?**], [15], the bistable pre-curved flapping wings in this study utilize PET layers as core layers instead of spring steel and replace the silicone fluidic actuation layer with McKibben artificial muscles, highly simplifying both the structural composition and manufacturing procedure as well as enhancing the actuator's overall flexibility and longevity.

B. *Fabrication and Prototyping*

The flapping wing is formed by sandwiching a PET core layer with a pair of prestressed 90° EMCs at a 60° angle. Here, 90° means the carbon fibers are aligned in the transverse direction of EMCs. The manufacturing process of EMCs can be found in [21]. The elastomer used for EMCs is Hongye E640 silicone rubber with a shore hardness of 40 HA. The wing is cut from a PET layer in a triangle shape. The proposed flapping-wing geometric parameters are illustrated in Fig. 2(a) and Table I. The following dimensions are defined for fabrication: PET layer's side length A_1, A_2 and A_3; EMCs' length L_1, L_2, and width d; and McKibben artificial muscles' length l_1, l_2 and diameter d_1; as well as snap rings' length m and width n.

Fig. 2(b) shows the fabrication steps for a flapping wing. Two EMCs are pre-stretched to a 45% prestrain along the ϵ_a and ϵ_b directions, respectively, and held by two clips. The two EMCs are then bonded to both sides of the PET layer using an instant adhesive (LOCTITE 401) along the pre-designed position as indicated by dashed frames, requiring a 30-minute curing time. Next, a pair of McKibben artificial muscles are

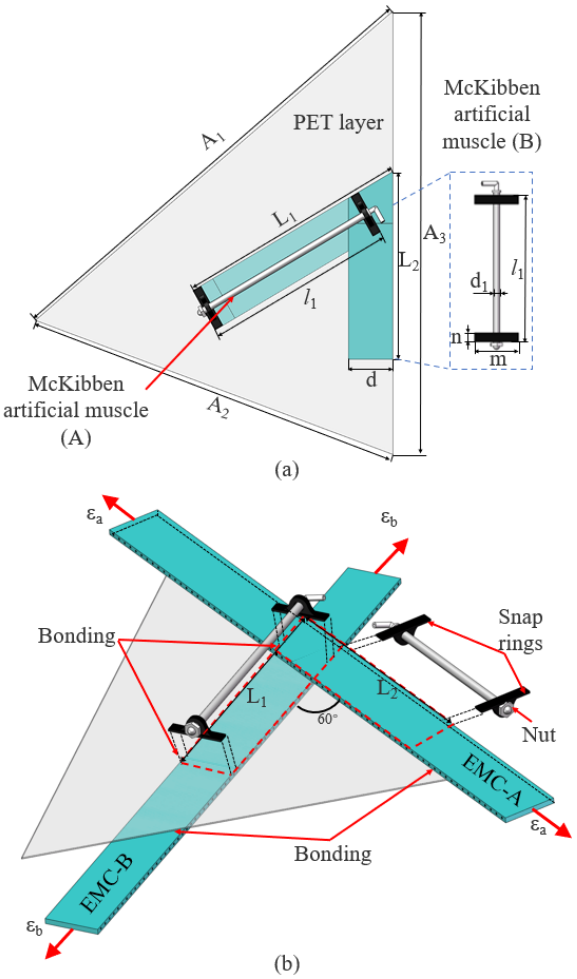

Fig. 2. (a) Geometry for a bistable pre-curved flapping wing. (b) The fabrication process of a bistable pre-curved flapping wing.

securely affixed to the opposite surfaces of the two EMCs via snap rings positioned at both termini. The snap rings are 3D printed utilizing an X1-Carbon Combo printer with polylactic acid with carbon fiber (PLA-CF), which are fastened in place using instant adhesive, with the nuts serving as a securing mechanism to prevent any inadvertent loosening. Two PVC pipe joints (Runze LD-016) are inserted into the McKibben artificial muscle air supply channels and linked to air supply tubes.

A connecting component, measuring 40x50x5 mm in dimensions, is 3D printed with PLA, which holds two symmetrically positioned flapping wings to constitute a bistable pre-curved swimming robot through its grooves on both sides. Instant adhesive is applied for enhancement to reinforce the connection.

TABLE I

GEOMETRIC PARAMETERS OF A FLAPPING WING (UNITS: MM).

A_1	A_2	A_3	L_1	L_2	d	l_1	l_2	d_1	m	n
210	171	193	100	85	20	85	75	3	20	3

C. Swimming Mechanism

Fig. 3 displays the time-lapse of the side and rear views of the robot using an iPhone 13 Pro, which shows seven representative shape variations within a pressurization and depressurization cycle, including a rapid upstroke (snap through, i–iv) and downstroke (snap back, iv-vii). Here, steps i and iv indicate the stable states II and I in Fig. 1, respectively. The pressure is set up as 350 kPa with a frequency of 2 Hz. Notably, the wingtip and center of mass (CoM) are highlighted with white and red circles, respectively.

Starting with stable state II, when pressurizing the pair of McKibben artificial muscles (A) on surface A, the bending stress in EMC-B is counteracted, triggering the robot to snap to stable state I (i–iv). Subsequently, the downstroke phase reverses this process (iv-vii): by pressurizing the pair of McKibben artificial muscles (B) on the surface B and depressurizing the muscles (A), the bending stress in EMC-A is counteracted, facilitating the robot's snap back to stable state II. The reciprocating oscillations from steps i to vii (bistable swimming mode) generate a staggered and closely spaced reverse Karman vortex street around the wing [22], [23]. This phenomenon causes the water behind it to move in a backward direction, resulting in a forward thrust for the robot. Whenever surface A or B is facing upwards, the robot moves forward, as defined as V in Fig. 1(b).

For the monostable mode, only the pair of muscles (A) are selected to be pressurized and depressurized at the shape of stable state I. The initial equilibrium state of the wing is pre-curved due to the prestress of the EMC. Pressurizing the McKibben artificial muscles increases the bending curvature along the direction of the motion V and depressurizing the muscles returns the flapping wing to its initial pre-curved state due to the stored elastic energy of the PET core layer. In contrast to the bistable swimming mode, the monostable mode has two propulsion directions by changing the orientation of surface A. When surface A is upward, the wings' tails generate forward thrust by flapping the water surface (V, see results in Section III-B). Whereas when surface A is downward, the monostable mode pushes the surrounding fluid forward, with the reaction forces propelling them to swim backward (-V, see demonstration in Section III-C), akin to the backward locomotion of a lobster. It's worth noting that the center of buoyancy and the CoM essentially coincide when swimming on the water's surface.

To generate turning motion, only one flapping wing is pressurized and depressurized no matter which surface is facing upwards, the asymmetrical thrust generates a moment around the CoM of the robot, yielding robot turning.

III. EXPERIMENTS AND DISCUSSION

To verify the swimming capabilities, dynamic experiments are conducted on the proposed robot. We first investigate the influence of pressure and actuation frequency changes on the robotic's propulsion speed when translating, considering both monostable (upstroke only) and bistable (completed upstroke to downstroke) actuation modes. Rotational tests are

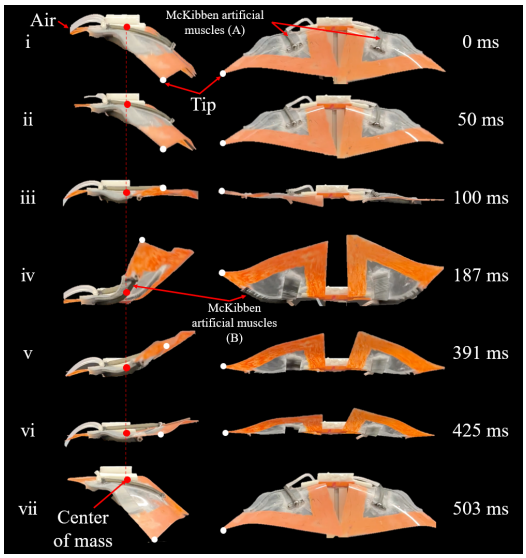

Fig. 3. The time-lapse images of pneumatically actuated motions during a representative cycle of upstroke [snap-through: i to iv] and downstroke [snap-back: iv and vii] wing flapping in both side view (left) and rear view (back) captured by an iPhone 13 Pro. The white and red circles denote the wing tip and the CoM of the swimming robot, respectively. Pressure is set as 350 kPa with a frequency 2 Hz.

conducted to evaluate the rotational angular velocity. Furthermore, flip-turning swimming underwater and transitioning from forward to backward swimming are demonstrated, which shows the robot's great performance for multimodal swimming.

A. Pneumatic Setup

An experimental pneumatic platform is established to assess the response of the swimming robot across varying pressure levels and actuation frequencies. Pneumatic pressure is supplied for the robot's inflation via an air pump and a set of pneumatic valves, which includes a pressure-regulating valve (AR2000), a throttle valve (ASC100-06), and solenoid valves (3V210-08-NC-A/B). Control signals are transmitted to these valves through an Arduino board featuring the Atmega328p CH340 microcontroller. The control strategy employed for the robotic is an open-loop approach, as detailed in [18].

B. Dynamic Tests of the Swimming Robot

Dynamic tests have been configured and executed on the swimming robot to quantify swimming velocity in relation to pressure and actuation frequency. Pneumatic pressure is administered to the robot via pulse-width-modulated (PWM) electromagnetic square wave signals characterized by diverse frequencies and pressures. The signal's duty cycle was fixed at 0.5.

The robot's responses to various actuation pressures are tested in both monostable and bistable modes when surface A faces upwards. The actuation frequency is set at 2 Hz. The bistability and monostability actuation step sequences are illustrated in Fig. 4. In the corresponding period, blue blocks indicate that a fixed pressure actuates the McKibben and remains constant, while white blocks indicate that the pressure is released to 0 kPa. Each block represents a quarter cycle. To quantify swimming speed, the robot is directed to perform ten cycles of PWM square wave motions under different pressures. Velocity is subsequently recorded by a NOKOV motion capture system. The number of measurements is three times for each pressure, taking the average values as the final results as shown in Fig. 5(a). It is observed that the higher the pressure, the faster the swimming velocity. Furthermore, it is noted that when the pressure falls below 300 kPa, the monostable and bistable modes' speeds are similar because the snap-through pressure of the bistable flapping wing is 300 kPa. Bistable mode completes only the upstroke at this moment and thus exhibits performance akin to that of monostable mode. Nevertheless, when the pressure is higher than 300 kPa, the bistable mode's velocity more than doubles that of the monostable mode, realizing a maximum swimming velocity of 12.23 mm/s (equivalent to 0.58 BL/s) at 400 kPa. This is due to the bistable mode's capability to finish the entire upstroke and downstroke under such conditions, effectively generating propulsion actions twice per cycle. Based on the tests, the Cost of Transport (CoT) [24] is utilized to quantify and evaluate the energy efficiency of the manta-ray-like robots. $CoT = W/(G * L)$ denotes the energy required for a transported object to move a specified distance forward, where W is the total input energy of the system, G is the total gravity of the system, and L is the system moves distance. The lower the CoT, the lower the energy consumption. The robotic achieved the lowest CoT of 13.87, which is far smaller than other swimmers [11], [25].

Subsequently, to investigate the speed response of the swimming robot to various actuation frequencies in a bistable mode, the pressure is set to 350 kPa, and the tracking results are depicted in Fig. 5(b) [see Supplementary Video S1]. It is observed that the robot's speed initially increases and then decreases, reaching its peak of 10.11 cm/s (equivalent to 0.48 BL/s) at approximately 2 Hz. This trend arises because frequency dominates the velocity changes in the frequency band below 2 Hz. However, when the frequency surpasses 2 Hz, the McKibben artificial muscles fail to track the pressure in this frequency range, which is due to extended dynamic response time attributed to fluid viscosity and long pneumatic line [17], [18]. In the following tests, 2 Hz frequency and 350 kPa pressure are used unless otherwise specified. The former ensures a relatively higher speed and the latter prevents damage to the artificial muscle from frequent use. Fig. 6 illustrates the robot translating 1 meter in monostable and bistable modes, respectively. The bistable swimming mode achieved more than twice the speed of the monostable mode.

Fig. 7 demonstrates the swimming robot executing a 180° clockwise rotation for monostable and bistable modes when surface A is oriented upwards. [Fig. 7(a) and (b), see Supplementary Video S2]. It is revealed that the robot rotates at angular velocities of 12°/s and 22.5°/s in monostable and bistable modes, respectively, for durations of 15 and 10 seconds, which is caused by propulsion actions twice per cycle for bistable modes. It is noted that the monostable

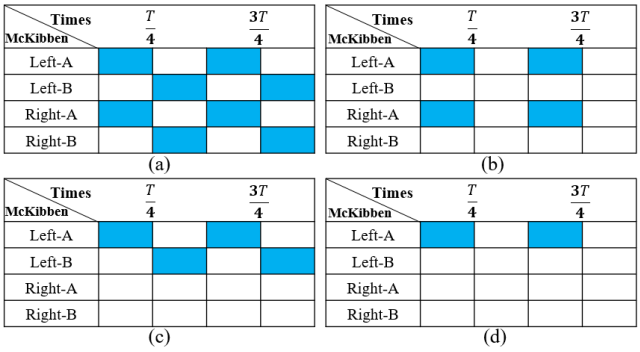

Fig. 4. Step cycle designed for (a) bistable and (b) monostable translating, (c) bistable and (d) monostable turning right. Left-A indicates the Mckibben on the left side of surface A, and other annotations follow similarly.

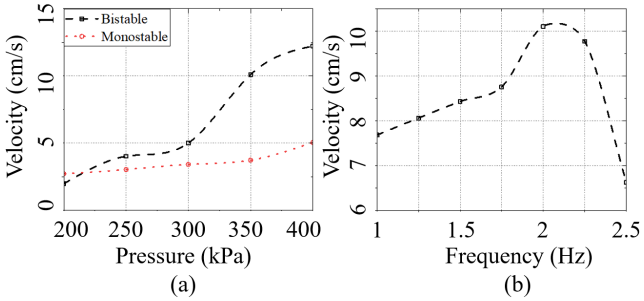

Fig. 5. (a) Velocity of the swimming robot for monostable and bistable modes versus pressure. (b) The velocity of the swimming robot for bistable mode versus frequency.

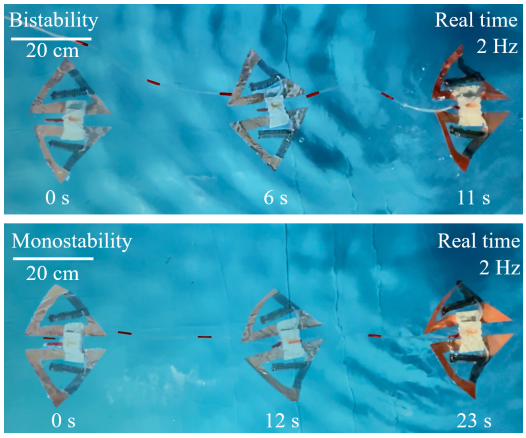

Fig. 6. Demonstration of bistable and monostable translating at a distance of 1 meter.

mode rotates almost in place, which is seldom seen in other studies, whereas the bistable mode features a rotation radius of about 19 cm, achieved through the greater centrifugal force produced by higher speed. Consequently, the monostable mode is better suited for narrow environments, while the bistable mode is more appropriate for scenarios requiring high-speed performance. The rotational angular velocity can be enhanced further by improving the pressure.

C. Multimodal Demonstration

The swimming robot is tested to demonstrate multimodal swimming capabilities with flip-turning and transitioning from forward to backward. Fig. 8(a) shows the robotic's

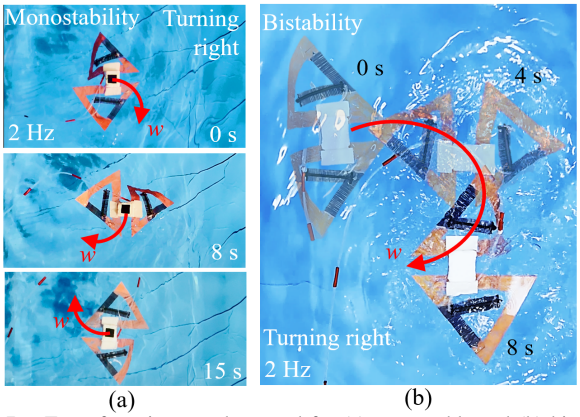

Fig. 7. Test of turning angular speed for (a) monostable and (b) bistable turning motion.

underwater flip-turning with upwards surface A (See Supplementary Video S3). To achieve buoyancy balance, a 30 g counterweight is incorporated, allowing controlled sinking and floating in the water. At lower actuation frequencies, the center of mass coincides with the center of buoyancy, ensuring stable locomotion underwater. However, with increased frequency, more flapping of wings causes instability of the robot and a separation between the center of gravity and buoyancy, producing an overturning moment. This enables the robot to transition from a horizontal to an upward inclination underwater and achieve the flip-turn maneuver with continuous actuation.

Fig. 8(b) exhibits the robot transitioning from forward to backward swimming on the water's surface without additional counterweights when surface A is oriented downwards. The robot is first set up in the bistable mode for 7 seconds to generate forward motion, then in the monostable mode for 11 seconds to translate backward to the original position. The principles for bistable and monostable swimming modes are detailed in Section II-C. These results effectively show the multi-modal swimming capabilities of the proposed swimming robot and display its extensive potential for applications in complex environments.

IV. CONCLUSIONS

This paper proposed a novel design of a high-performance manta ray-inspired robot utilizing bistable flapping wings composed of prestressed composite and McKibben artificial muscles. Dynamic experiments were conducted and showed that the robot achieved the maximum translating speed of 0.58 BL/s, and turning speed of 22.5 °/s for bistable modes, yielding more than twice those speeds of monostable mode. Moreover, the slow speed of the monostable mode resulted in a small turning radius, enabling in-place rotation.

Furthermore, compared to previous studies which only can achieve swimming and turning [8], [9], [12], the proposed robot was shown to achieve multimodal swimming, including forward and backward translating, turning, and flip-turning. It was found that alternating bistable to monostable mode results in forward and backward motion. Hence, allowing transitioning from forward to backward swimming in place.

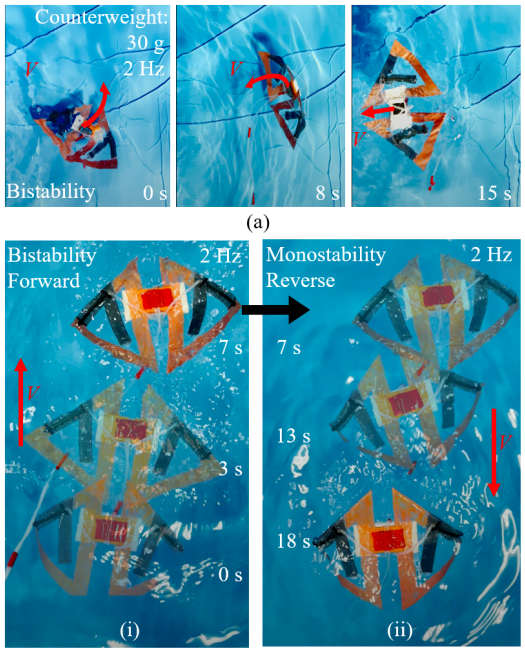

Fig. 8. Multimodal locomotion based on bistable robotics (a) Demonstration of flip-turning swimming. (b) Demonstration of transitioning from forward to backward swimming through bistable to monostable mode.

Rotations in place and out of place were realized by the monostable and bistable modes, respectively. The former was due to the reduced centrifugal force resulting from the lower monostable mode propulsion speed, occurring once per cycle. Furthermore, flip-turning swimming modes were achieved by an overturning moment created by the separation between the CoM and the center of buoyancy.

This study offers a new paradigm for designing manta-ray-like robots with high-speed and multi-modal swimming capabilities. Further efforts include the untethered design of the robot for free-water swimming and improving the robot's swimming energy efficiency compared to the actual efficiency of manta rays. Furthermore, we will achieve integrated drive and control. Additionally, dynamic modeling and model-based parametric studies of the swimming robot will be conducted to maximize efficiency and ensure precise control.

REFERENCES

[1] F. E. Fish, C. M. Schreiber, K. W. Moored, G. Liu, H. Dong, and H. Bart-Smith, "Hydrodynamic performance of aquatic flapping: efficiency of underwater flight in the manta," Aerospace, vol. 3, no. 3, p. 20, 2016.

[2] C. W. Zhang, W. Zou, H. C. Yu, X. P. Hao, G. Li, T. Li, W. Yang, Z. L. Wu, and Q. Zheng, "Manta ray inspired soft robot fish with tough hydrogels as structural elements," ACS Applied Materials & Interfaces, vol. 14, no. 46, pp. 52430–52439, 2022.

[3] Z. Lv, Z. Wang, Y. Lv, and M. Yuan, "An airsea manta-ray robot in 5g ogce," in Proceedings of the 2019 2nd International Conference on Service Robotics Technologies, pp. 63–67, 2019.

[4] G. Li, Y. Deng, O. L. Osen, S. Bi, and H. Zhang, "A bio-inspired swimming robot for marine aquaculture applications: From concept-design to simulation," in OCEANS 2016-Shanghai, pp. 1–7, IEEE, 2016.

[5] D. Zhang, G. Pan, Y. Cao, Q. Huang, and Y. Cao, "A novel integrated gliding and flapping propulsion biomimetic manta-ray robot," Journal of Marine Science and Engineering, vol. 10, no. 7, p. 924, 2022.

[6] J. He, Y. Cao, Q. Huang, Y. Cao, C. Tu, and G. Pan, "A new type of bionic manta ray robot," in Global Oceans 2020: Singapore–US Gulf Coast, pp. 1–6, IEEE, 2020.

[7] Q. Liu, H. Chen, Z. Wang, Q. He, L. Chen, W. Li, R. Li, and W. Cui, "A manta ray robot with soft material based flapping wing," Journal of Marine Science and Engineering, vol. 10, no. 7, p. 962, 2022.

[8] J. Wang, Q. Liu, H. Cheng, B. Fang, J. Zhang, and J. Hong, "Design, fabrication and experiment of a bionic manta ray robot fish," in 2022 IEEE International Conference on Robotics and Biomimetics (ROBIO), pp. 2195–2200, IEEE, 2022.

[9] Y. Sun, H. Feng, X. Liang, A. J. Goh, P. Qi, M. Li, M. H. Ang Jr, and R. C. Yeow, "Powerful 2d soft morphing actuator propels giant manta ray robot," Advanced Intelligent Systems, vol. 4, no. 11, p. 2200186, 2022.

[10] Y. Zhao, Q. Li, Z. Liu, Y. Alsaid, P. Shi, M. Khalid Jawed, and X. He, "Sunlight-powered self-excited oscillators for sustainable autonomous soft robotics," Science Robotics, vol. 8, no. 77, p. eadf4753, 2023.

[11] Y. Chi, Y. Hong, Y. Zhao, Y. Li, and J. Yin, "Snapping for high-speed and high-efficient butterfly stroke–like soft swimmer," Science Advances, vol. 8, no. 46, p. eadd3788, 2022.

[12] J. C. Osorio, C. Tinsley, K. Tinsley, and A. F. Arrieta, "Manta ray inspired multistable soft robot," in 2023 IEEE International Conference on Soft Robotics (RoboSoft), pp. 1–6, IEEE, 2023.

[13] Y. Chi, Y. Tang, H. Liu, and J. Yin, "Leveraging monostable and bistable pre-curved bilayer actuators for high-performance multi-task soft robots," Advanced Materials Technologies, vol. 5, no. 9, p. 2000370, 2020.

[14] D. K. Patel, X. Huang, Y. Luo, M. Mungekar, M. K. Jawed, L. Yao, and C. Majidi, "Highly dynamic bistable soft actuator for reconfigurable multimodal soft robots," Advanced Materials Technologies, vol. 8, no. 2, p. 2201259, 2023.

[15] Y. Zhou and Z. Xu, "Mechanically Prestressed Pneumatically Driven Bistable Soft Actuators," Journal of Mechanisms and Robotics, vol. 16, p. 051006, 07 2023.

[16] Z. Xu and Y. Zhou, "Bistable composites with intrinsic pneumatic actuation and non-cylindrical curved shapes," Materials Letters, vol. 354, p. 135381, 2024.

[17] Z. Xu, L. Hu, L. Xiao, H. Jiang, and Y. Zhou, "Modular soft robotic crawlers based on fluidic prestressed composite actuators," Journal of Bionic Engineering, vol. 21, no. 2, pp. 694–706, 2024.

[18] Z. Xu, L. Hu, and Y. Zhou, "A soft gripper integrated with mechanically-prestressed soft actuators," in 2022 IEEE International Conference on Sensing, Diagnostics, Prognostics, and Control (SDPC), pp. 190–194, IEEE, 2022.

[19] A. Pagoli, F. Chapelle, J.-A. Corrales-Ramon, Y. Mezouar, and Y. Lapusta, "Review of soft fluidic actuators: Classification and materials modeling analysis," Smart Materials and Structures, vol. 31, no. 1, p. 013001, 2021.

[20] Y. Zhou, L. M. Headings, and M. J. Dapino, "Modeling of soft robotic grippers integrated with fluidic prestressed composite actuators," Journal of Mechanisms and Robotics, vol. 14, no. 3, 2022.

[21] Y. Zhou, L. M. Headings, and M. J. Dapino, "Modeling of fluidic prestressed composite actuators with application to soft robotic grippers," IEEE Transactions on Robotics, 2022.

[22] D. Lentink, F. T. Muijres, F. J. Donker-Duyvis, and J. L. Van Leeuwen, "Vortex-wake interactions of a flapping foil that models animal swimming and flight," Journal of Experimental Biology, vol. 211, no. 2, pp. 267–273, 2008.

[23] G. S. Triantafyllou, M. S. Triantafyllou, and M. A. Grosenbaugh, "Optimal thrust development in oscillating foils with application to fish propulsion," Journal of Fluids and Structures, vol. 7, no. 2, pp. 205–224, 1993.

[24] Y. Dal Jeong, M. J. Kim, and J. H. Lee, "Intermittent swimming of two self-propelled flexible fins with laterally constrained heaving motions in a side-by-side configuration," Journal of Fluid Mechanics, vol. 960, p. A39, 2023.

[25] C. Christianson, C. Bayag, G. Li, S. Jadhav, A. Giri, C. Agba, T. Li, and M. T. Tolley, "Jellyfish-inspired soft robot driven by fluid electrode dielectric organic robotic actuators," Frontiers in Robotics and AI, vol. 6, p. 126, 2019.